



Synthesis of ultrathin hollow carbon shell from petroleum asphalt for high-performance anode material in lithium-ion batteries



Peng Li^a, Jingyan Liu^a, Yuwei Wang^b, Yang Liu^a, Xiuna Wang^b, Kyung-Wan Nam^c, Yong-Mook Kang^c, Mingbo Wu^{a,*}, Jieshan Qiu^{b,*}

^aState Key Laboratory of Heavy Oil Processing, China University of Petroleum, Qingdao 266580, China

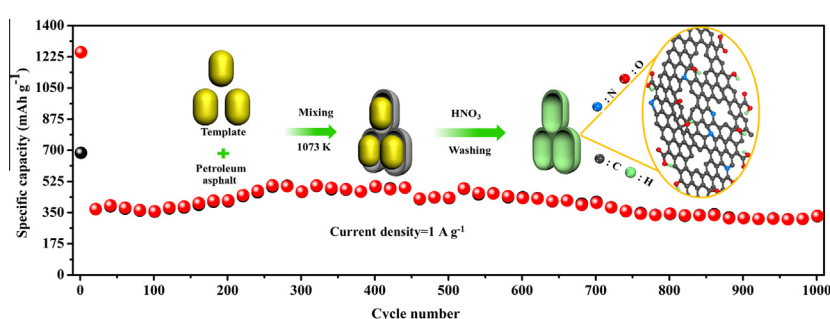
^bState Key Laboratory of Fine Chemicals, School of Chemical Engineering, Dalian University of Technology, Dalian 116024, China

^cDepartment of Energy and Materials Engineering, Dongguk University-Seoul, Seoul 100-715, Republic of Korea

HIGHLIGHTS

- A facile template-assisted method has been proposed to prepare hollow carbon shell.
- Ultrathin hollow carbon shell was unprecedentedly prepared from petroleum asphalt.
- The ultrathin carbon shell shortens the distance of ion diffusion to less than 2.5 nm.
- Hollow carbon shell shows a capacity of 334 mA h g⁻¹ after 1000 cycles at 1 A g⁻¹.

GRAPHICAL ABSTRACT



ARTICLE INFO

Article history:

Received 4 September 2015

Received in revised form 22 October 2015

Accepted 29 October 2015

Available online 6 November 2015

Keywords:

Carbon materials
Energy storage and conversion
Carbon shell
Petroleum asphalt
Lithium-ion battery

ABSTRACT

Petroleum asphalt based ultrathin hollow carbon shell (PACS) was prepared via a facile template-assisted method. As the anode material of lithium-ion batteries, PACS exhibits high reversible capacity, excellent cycling stability, and superior rate performance. A high reversible capacity of 334 mA h g⁻¹ and 90% kept of the theoretical capacity can still be maintained in PACS at a current density of 1 A g⁻¹ even after 1000 cycles, which is ascribed to the unique hollow structure, ultrathin porous shells (4.7 nm), the doped nitrogen atoms, and high level of disorder degree. Meanwhile, the present study paves a milestone for the high-valued utilization of petroleum asphalt and other kinds of heavy oil.

© 2015 Elsevier B.V. All rights reserved.

1. Introduction

The demand for rechargeable batteries in hybrid electric vehicles, communication devices, portable electronics and other renewable energy storages has sparked efforts in exploring Li-ion batteries (LIBs) with high specific capability, charging stability and rate capability [1–3]. With satisfying stability,

graphite has been normally used as the commercial anode material, however, it can hardly meet the ever-increasing demand on account of the limited theoretical capacity (372 mA h g⁻¹). Quantities of attempts have been made to explore or design novel nanostructures of electrode materials to meet the demand, and some elements or compounds (e.g. Sn, Sb, Si or Ge) have been alloyed with lithium to further increase LIB's capacity [4]. Nevertheless, huge volume change in alloying electrodes or large voltage hysteresis in conversion electrodes severely hinders their application in LIBs [5,6].

* Corresponding authors.

E-mail addresses: wumb@upc.edu.cn (M. Wu), jqu@dlut.edu.cn (J. Qiu).

Till now, numerous novel carbon-based LIB electrode materials with various kinds of microstructures have been investigated, e.g. carbon nanotube [7], carbon nanobead [8], ordered mesoporous carbon [9], graphene [10], and their composites [11], among which hollow carbon materials (HCMs) has been demonstrated to be desirable for large volume change accommodation, extra Li ion storage space, short solid-state diffusion and charge-transfer rate [12–14]. Tien et al. synthesized uniform carbon spheres with a good specific capacity above 330 mA h g^{-1} after 130 cycles [12], and the novel hollow carbon cage/graphene nanocomposite prepared by catalytic decomposition of xylene on MgO supported Co and Mo catalyst achieved a reversible capacity of 574 mA h g^{-1} at a current density of 100 mA g^{-1} after 60 discharge/charge cycles [13]. Crystalline carbon hollow spheres synthesized by Jim et al. exhibited a stable capacity about 300 mA h g^{-1} after 200 cycles [14].

Petroleum asphalt, as a by-product of vacuum distillation of crude oil, has been mostly employed as fuel or binder in road construction and roofing field, and the low-level utilization is a great waste of resources. Besides, the recent global economic downturn has caused massive investment curtailment on construction, further worsening the overcapacity of petroleum asphalt. So, it is urgent to fulfill the high-value utilization of petroleum asphalt. Actually, petroleum asphalt with high content of aromatic hydrocarbons is a promising raw material to prepare HCMs through aromatization and carbonization [15]. Although, Wei et al. successfully obtained graphene from petroleum asphalt with vermiculite as the direct template [15], the removal of vermiculite is time consuming and the yield of final graphene is apparently unfavorable. Cheng et al. prepared graphene like carbon paper through pyrolyzing petroleum asphalt with a piece of glass covered on the top [16], but the obtained carbon paper is too thick (ca. $1 \mu\text{m}$) to show satisfactory lithium storage performance. Obviously, a facile and

effective way is needed to further enhance the utilization of petroleum asphalt in LIBs.

Herein, we developed a facile template-assisted method to fabricate ultrathin hollow carbon shell from petroleum asphalt (PACS). It is noted that the as-made PACS with hollow structure and ultrathin shell can be endowed with several advantages as LIB anode, e.g. short ion diffusion length and convenient electronic transmission path. As expected, PACS exhibits an excellent electrochemical performance as an anode material for LIBs.

2. Experimental

2.1. Synthesis

Petroleum asphalt from China National Offshore Oil Corp. (17.63 wt% of saturates, 31.13 wt% of aromatics, 38.21 wt% of resins and 6.40 wt% of asphaltenes) was used as the carbon precursor. In a typical process, 5 g of black petroleum asphalt was added to 100 mL toluene followed by sonication for 30 min. 15 g of commercial ZnO nanoparticles ($90 \pm 10 \text{ nm}$ in size) purchased from Aladdin (Shanghai, China) was added to the obtained suspension under stirring, and the resulting mixture was dried at 373 K under stirring in oil bath to obtain brown mixture which was then heated at 1073 K for 1 h under nitrogen atmosphere. The prepared product (named ZnO@PACS) was sufficiently washed with 4 M nitric acid and distilled water, and finally dried at 373 K. The obtained sample is denoted as PACS. Moreover, pure graphite, bare petroleum asphalt carbon (BPAC) and ZnO@PACS, which were prepared by the same procedure except for the removal of template, were used for comparison. To investigate whether 1073 K is suitable for PACS to be utilized in LIBs, P600 (873 K) and P1000 (1273 K) were also obtained through similar progress.

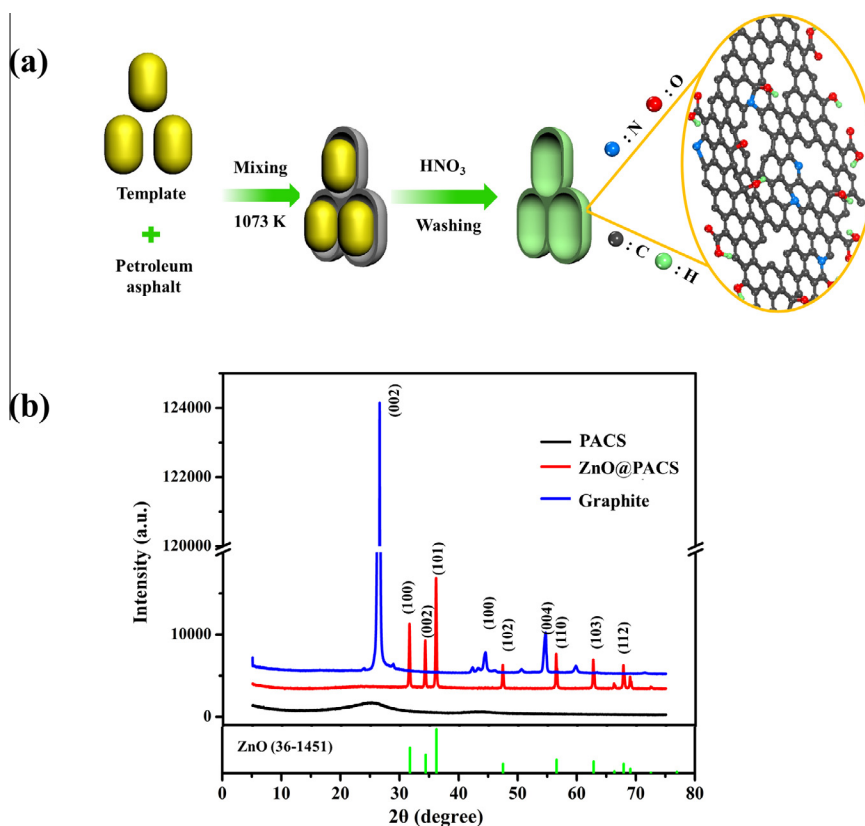


Fig. 1. (a) Synthesis schematic for PACS; (b) XRD patterns of PACS, ZnO@PACS and graphite.

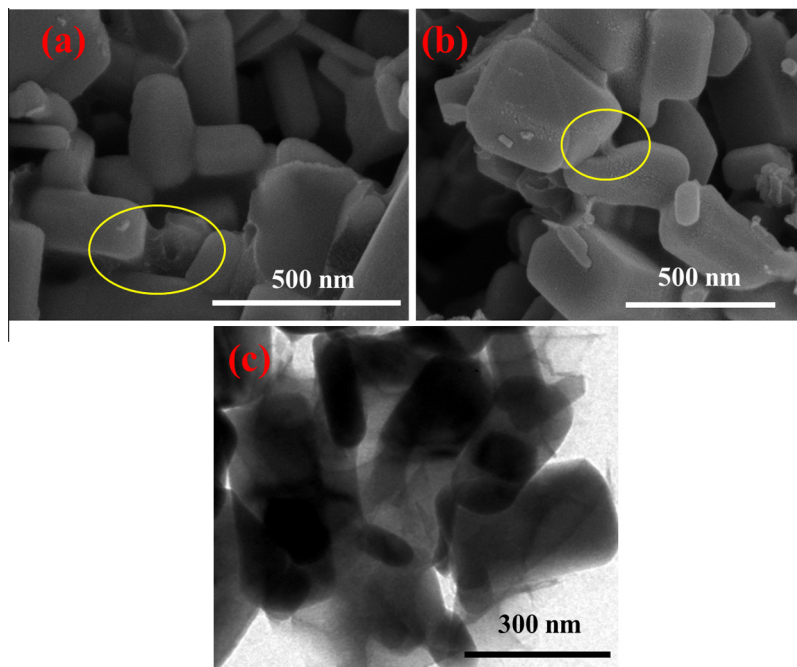


Fig. 2. (a) and (b) SEM and (c) TEM images of ZnO@PACS.

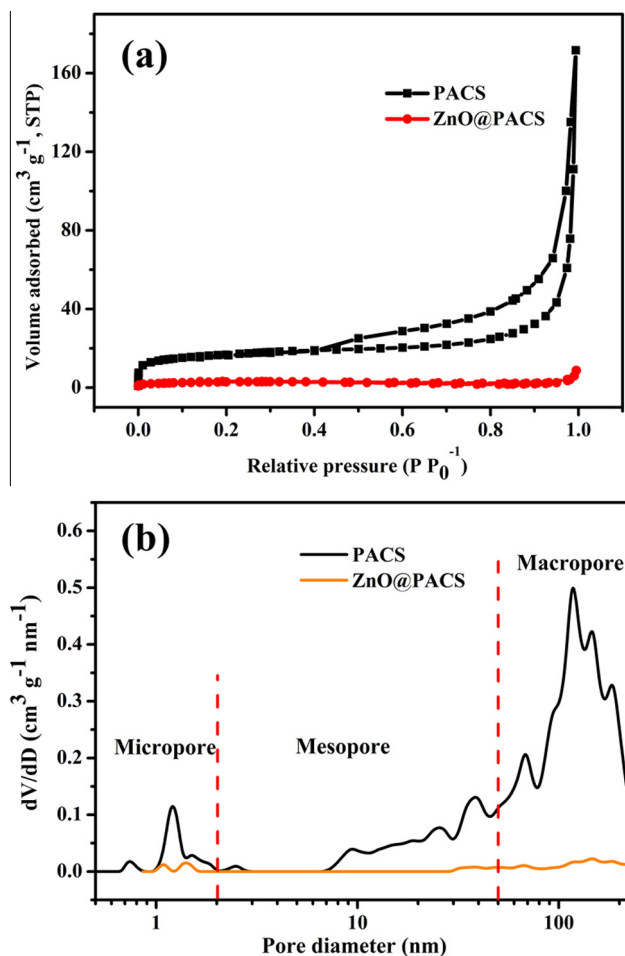


Fig. 3. (a) N_2 adsorption–desorption isotherms and (b) pore size distribution of PACS and ZnO@PACS.

2.2. Characterization

As-prepared products were characterized with X-ray diffraction (XRD) (X'Pert PRO MPD, Holland) using Cu $K\alpha$ radiation ($\lambda = 1.518 \text{ \AA}$). The pore structure was tested by low temperature nitrogen adsorption–desorption isotherms on a sorptometer (Micromeritics, ASAP 2020, America) using the Brunauer–Emmett–Teller (BET) method. Transmission electron microscopy (TEM) (JEM-2100UHR, Japan) was applied to investigate the morphology and microstructure of obtained samples. The crystallinity of as-made samples was labeled by Raman analysis carried out by a Jobin–Yvon Labram-010 Raman spectrometer.

2.3. Electrochemical measurements

The obtained sample, carbon black and poly(vinylidene) fluoride (PVDF) binder were mixed and dissolved in N-methyl-2-pyrrolidinone at the weight ratio of 8:1:1 to make well-mixed slurry, which was coated on a copper foil current collector and vacuum dried at 373 K for 8 h. Then CR2032 coin cells were assembled in an Ar-filled glove box, with the as-obtained material as working electrode, lithium foil as counter and reference electrode, polypropylene film as the separator, and 1 M $LiPF_6$ in a 1:1 (v/v) mixture of ethylene carbonate and dimethyl carbonate (EC/DMC) as the electrolyte. The cells were galvanostatically charge-discharged between 0.005 and 3 V vs. Li/Li^+ on a Land CT2001A battery test system. Electrochemical impedance spectroscopy (EIS) tests were also tested by Ametek PARSTAT4000 electrochemistry workstation in the frequency range of 100 kHz–10 mHz with AC voltage amplitude of 10 mV.

3. Results and discussion

Fig. 1(a) describes the overall synthesis process of PACS. During the heat-treatment process, petroleum asphalt melts and uniformly envelops ZnO templates with thin carbon layer before condensation. Afterwards, the mixture is carbonized at 1073 K for 1 h. With the assistance of nitric acid solution, the metal oxide

templates are easily and thoroughly removed, leaving PACS with size-controllable holes and ultrathin carbon shell, and the yield of PACS in a typical run is about 22%. Fig. 1(b) shows the XRD patterns of ZnO@PACS, PACS and graphite, respectively. The sharp peaks of ZnO@PACS can be indexed to the wurtzite-type hexagonal ZnO (JCPDS, No. 36-1451). Besides, only two diffraction peaks around 24° and 43° corresponding to (002) and (100) planes of graphitic carbon can be observed from the XRD pattern of PACS, indicating that all ZnO nanotemplates have been removed by the nitric acid solution. Notably, peaks of PACS are much broader compared with the sharp ones of graphite, demonstrating an apparent amorphous carbon structure of PACS with lower crystallinity.

Fig. 2 shows the morphology and microstructure of ZnO@PACS. The cobweb-like material in the yellow circle (Fig. 2(a) and (b)) might be the ultrathin carbon layer coating the ZnO templates. Fig. 2(c) further demonstrates that there is a relatively uniform coating of petroleum asphalt based carbon on ZnO.

To further examine the porous structure of PACS and ZnO@PACS, nitrogen adsorption–desorption analysis was measured. As shown in Fig. 3(a), according to IUPAC classification method, the isotherm of PACS has a typical type IV shape with a type H3 hysteresis located at a relative pressure of 0.41–0.95, confirming the existence of mesoporous structure [17]. Besides the mesopores, PACS also possesses some micropores and abundant macropores as shown in Fig. 3(b). Nevertheless, there is seldom porous structure in ZnO@PACS and the specific surface area is only $10.4 \text{ m}^2 \text{ g}^{-1}$. Mesopores and macropores formed in PACS could be ascribed to the removal of ZnO template via acid wash, while micropores might arise from the vaporization of volatile materials in petroleum pitch. Such a hierarchical porous microstructure with specific surface area around $188 \text{ m}^2 \text{ g}^{-1}$ can not only provide abundant active sites for the insertion and storage of Li^+ but also improve the accessibility of the active sites to Li^+ [18].

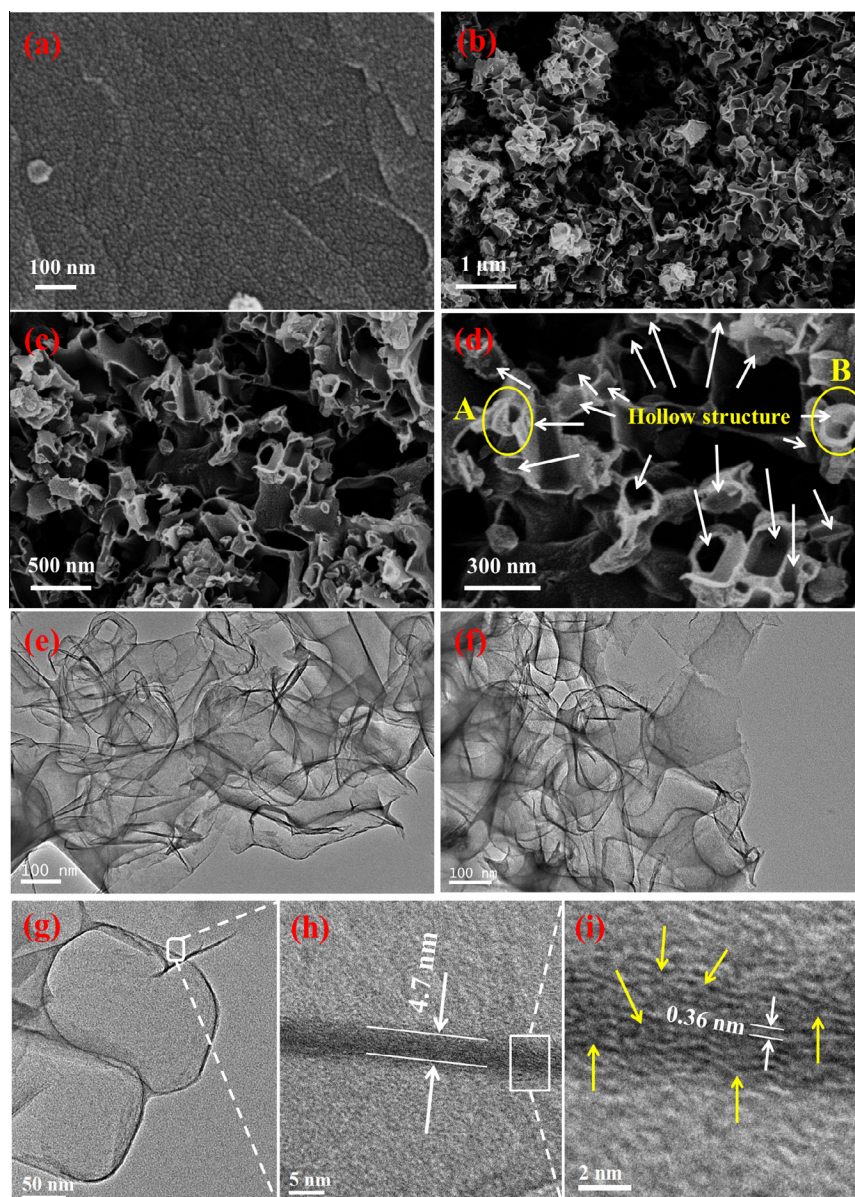


Fig. 4. SEM images of (a) BPAC and (b)–(d) PACS; (e)–(g) TEM image and (h) and (i) HR-TEM images of as-prepared PACS. (For interpretation of the references to color in this figure legend, the reader is referred to the web version of this article.)

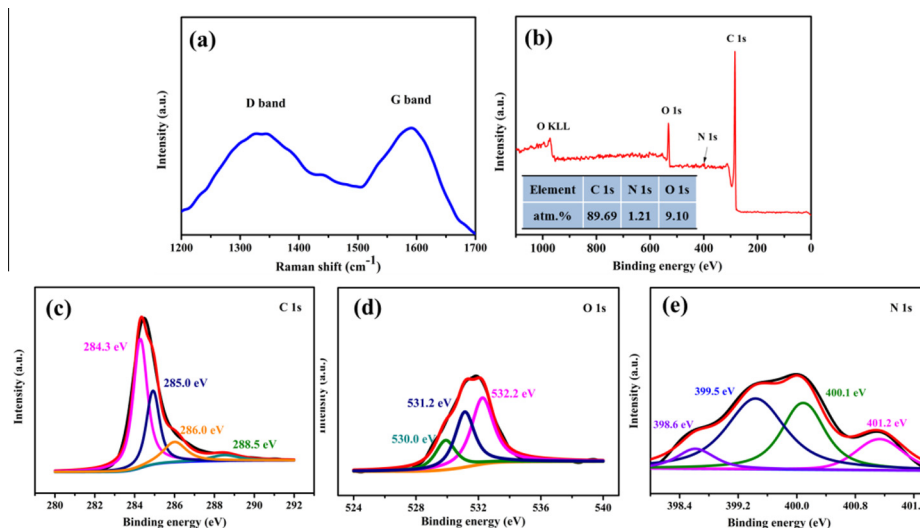


Fig. 5. (a) Raman spectrum and (b) XPS spectrum of PACS; XPS spectra of (c) C 1 s, (d) O 1 s and (e) N 1 s regions of PACS.

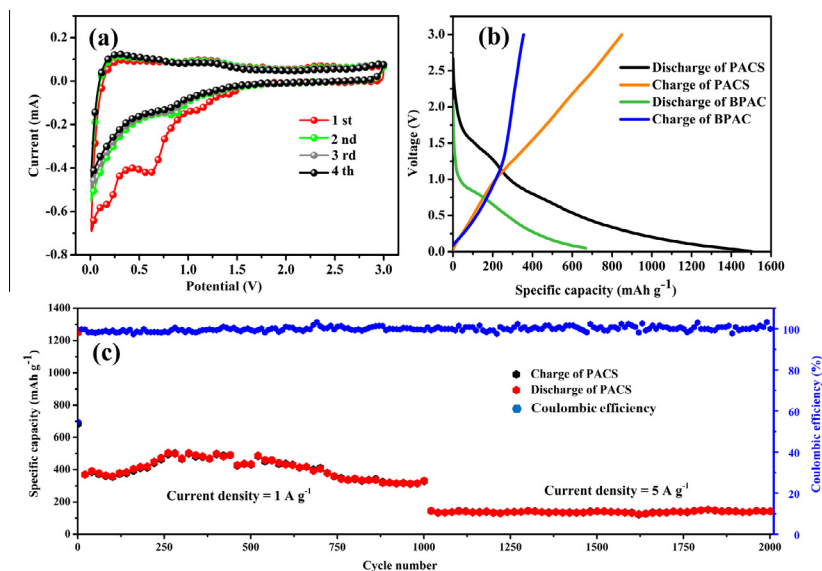


Fig. 6. (a) Cyclic voltammetry curve of PACS; (b) first discharge/charge profiles of PACS and BPAC at a current density of 100 mA g^{-1} ; (c) cycling performance of PACS at 1 and 5 A g^{-1} .

SEM and TEM images are also used to investigate the microstructure and morphology characteristics of as-prepared samples. Compared with the smooth surface of BPAC (Fig. 4(a)), the SEM image of PACS (Fig. 4(b)–(d)) clearly shows the unique three-dimensional hierarchical porous structure, in which the macropores can play a role of ion-buffering reservoirs thus making sure that almost every part of the PACS structure could be immersed in the electrolyte. As shown in Fig. 4(d), there are abundant hollow structures (white arrows). The hollow structures (circles A and B) with breakages ploughing out and collapsing can be obviously identified. Besides, Fig. 4(e) and (f) also exhibit carbon shells with apparent hollow structure. In Fig. 4(g) and (h), the uniform and ultrathin thickness (about 4.7 nm) might be the most attractive feature of nanotemplate-assisted formed PACS, i.e. the ion diffusion distance could be shortened to less than 2.5 nm, ideal for the adsorption of lithium ions in organic electrolyte. In Fig. 4(i), the lattice spacing of PACS (0.360 nm) is larger than 0.335 nm of

(002) plane for graphite, validating the low graphitization degree of as-prepared PACS. The discontinuous graphitic layers and numerous defects (yellow arrows) in PACS, which can provide additional intercalation sites, are propitious to the storage and diffusion of lithium ions [19]. This explanation can be further confirmed by Raman spectra (Fig. 5(a)). As shown in Fig. 5(a), G band (around 1585 cm^{-1}) corresponds to the sp^2 -bonded carbon atoms, while D band (near 1340 cm^{-1}) is related to the disordered carbons [20,21]. The intensity ratio (I_D/I_G) of PACS is about 0.93, indicating the disordered carbon structure. So it is highly plausible that PACS may exhibit unusual electrochemical performance when utilized as anode material for LIBs.

XPS analysis was conducted to further analyze the elemental composition of PACS. The full-range XPS spectrum of PACS in Fig. 5(b) shows C 1s peak at ca. 284.5 eV, O 1s peak at ca. 531.7 eV and N 1s peak at ca. 400.0 eV, corresponding to 89.69%, 9.10% and 1.21% of atom contents, respectively. In Fig. 5(c), peaks

at 284.3 and 286.0 eV are attributed to C–C groups of graphite and C–O groups, respectively [22]. Besides, C–N bond (285.0 eV) originating from N substitution and defects or the edge of PACS is obviously identified, which is consistent with previous reports [23]. Taking the high electronegativity of N atoms into account, the peak centered at 288.5 eV should correspond to other binding configurations such as O–C=O formed at the edge of PACS [24]. O 1s spectra of PACS shown in Fig. 5(d) indicate the existence of oxygen-containing functional groups, i.e. C=O, C–OH and COOH. As seen in Fig. 5(e), there are three kinds of N in PACS, i.e. pyridine-like N (398.6 eV), pyrrolic N (399.5 and 400.1 eV) and graphite-like N (401.2 eV) [24,25]. The incorporated nitrogen atoms introduce lots of defects and enhance the binding with lithium ions, relatively favorable to lithium storage capacity [26].

The cyclic voltammetry curve of PACS (Fig. 6(a)) demonstrates three peaks at 1.2, 0.6 and 0.01–0.2 V in the first reduction process. The small peak at 1.2 V is due to the reaction of lithium with functional groups at the carbon surface, e.g. oxygen containing functional groups depicted in Fig. 5(d) [27], whereas the intensive peak at 0.6 V corresponds to formation of SEI film and the decomposition of electrolyte during the first discharge process [28]. The 0.01–0.2 V peak can be attributed to the reversible insertion of Li into the graphite layers and the nanocavities [29,30]. In the subsequent delithiation process, the broad oxidation peaks at 0.2 and ca. 1.2 V are related to the Li-extraction from the graphite layers and the extraction from the nanocavities, respectively [30]. The voltage profile looks very similar with that of amorphous carbon, which is consistent with the result of Fig. 1(b).

In order to confirm that the calcination temperature (1073 K) is suitable for lithium storage, the charge/discharge specific capacities of samples obtained at different temperature were investigated as shown in Fig. S1. The discharge specific capacity of P1000 (212 mA h g⁻¹) after 170 cycles is lower than 421 mA h g⁻¹ of PACS, owing to the excessive graphitization, which is consistent with previous works [28]. Besides, P600 also shows a relatively lower specific capacity (289 mA h g⁻¹) compared with 421 mA h g⁻¹ of PACS, which might be attributed to the insufficient formation of conductive framework [31] and relatively low electrochemical activity, confirmed by EIS test in Fig. 7.

Fig. 6(b) depicts the first discharge/charge profiles of PACS and BPAC at a discharge/charge rate of 100 mA g⁻¹. The as-obtained PACS delivers a discharge/charge capacity of 1502/848 mA h g⁻¹, much higher than 668/356 mA h g⁻¹ of BPAC, due to the distinct microstructures between PACS and BPAC. In BPAC, there is no developed pore-system but compact carbon blocks, which is unfavorable to the fast transport of Li⁺. In PACS, the unique carbon shell with nano-sized thickness and carbon skeleton sustained by plentiful pores intensively facilitate the insertion and extraction of Li⁺. Besides, micropores and part of mesopores may also provide sites for lithium storage.

In order to evaluate the cycling performance of PACS as anode for LIBs, galvanostatic discharge–charge test was performed in the voltage window of 0.005–3.0 V at current densities of 1 and 5 A g⁻¹ (Fig. 6(c)). There is a large irreversible capacity and low initial coulombic efficiency (around 55%) in the first discharge–charge process, which is a common phenomenon for carbon-based materials due to the formation of SEI film [14]. The specific capacity of PACS anode is stable and reversible after the initial few cycles, then slowly rises to 485 mA h g⁻¹ after 400 cycles at the current density of 1 A g⁻¹ in consequence of the activating process of the porous anode [32,33]. More interestingly, a stable specific capacity of 334 mA h g⁻¹ (ca. 90% of the theoretical capacity of graphite, i.e. 372 mA h g⁻¹) can still be maintained even after 1000 cycles, and the coulombic efficiencies approach 100% after the second cycle. The cycling performance of PACS was also tested under a current density of 5 A g⁻¹ after 1000 charge–discharge cycles at 1 A g⁻¹.

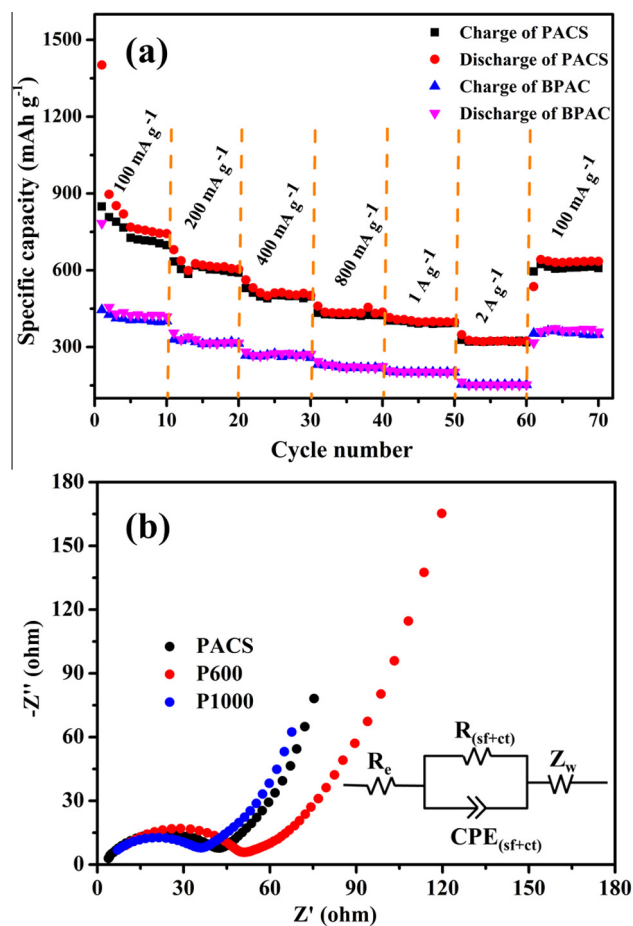


Fig. 7. (a) Rate performance of PACS and BPAC; (b) Nyquist plots and the equivalent circuit for PACS, P600 and P1000.

Table 1

Comparison of the lithium storage performance of various carbon materials.

Sample	Current density (mA g ⁻¹)	Capacity (mA h g ⁻¹)	Refs.
Interconnected hollow carbon nanospheres	744	337	[4]
Nanoporous graphene sheets	1000	256	[34]
Porous carbon obtained by incorporating silica into benzoxazine	1000	280	[18]
Carbon nanotube film	744	200	[35]
PACS	1000	334	Our work

The lithium storage property rarely decreases. A specific capacity of 142 mA h g⁻¹ is expectedly maintained after 1000 cycles at 5 A g⁻¹, demonstrating an excellent cycling performance and impressing structural stability of PACS. Nevertheless, BPAC and ZnO@PACS as anode materials exhibit only 176 and 51 mA h g⁻¹ respectively at a current density of 1 A g⁻¹ after 100 cycles (Fig. S2 (a) and (c)). Besides, BPAC tested under a current density of 5 A g⁻¹ after 100 charge–discharge cycles at 1 A g⁻¹ exhibits 70.8 (first cycle) and 33.3 mA h g⁻¹ (100th cycle), exhibiting poor cycling stability, as shown in Fig. S2(b). To our knowledge, the excellent lithium storage property of as-obtained PACS is higher than many reported carbon-based anodes (Table 1) [4,18,34,35].

Importantly, PACS anodes also exhibit remarkable rate capability compared with that of BPAC (Fig. 7(a)). The reversible specific



Fig. 8. Schematic of lithium storage and transport in PACS.

capacities of PACS anodes are 730, 621, 511, 432, 398 and 324 mA h g⁻¹ at 100, 200, 400, 800, 1000 and 2000 mA g⁻¹, respectively, which are much superior to those of BPAC (Fig. S3). Once the current density is tuned back to 100 mA g⁻¹, the specific capacity of PACS electrode can still recover to 632 mA h g⁻¹.

Electrochemical impedance spectroscopy (EIS) tests were performed to explore the effect of the calcination temperature on the electronic conductivity (Fig. 7(b)), and ensure the microstructure stability (Fig. S4). The intercept at the real impedance axis in the high frequency area indicates the ohmic resistance (R_e), which is related to the total resistance of the electrolyte, separator and electrical contacts, and the diameter of the semicircle represents the charge-transfer resistance (R_{ct}) and the Li⁺ migration resistance through the SEI film (R_{sf}) [31,36,37]. As shown in Fig. 7(b), the $R_{(sf+ct)}$ of P600 (50.8 Ω) is much bigger than 38.1 Ω of PACS, which is marginally bigger than 32.4 Ω of P1000, confirming the low electrochemical activity of P600 [38]. In Fig. S4, the $R_{(sf+ct)}$ after 1000 cycles is 40.3 Ω, similar with that (38.1 Ω) after just one cycle, showing an excellent cycling stability of PACS.

Fig. 8 illustrates the schematic of Li ion storage and transport mechanism within PACS. The excellent electrochemical properties of the carbon shells obtained through a facile template-assisted method in this work are attributed to the hierarchical architecture, which can store a great amount of lithium ions apart from the general insertion and surface adsorption, and virtually facilitates the fast distribution of ions and electrolyte. Besides, the well-contacted carbon shells with apparent graphitic layers also largely promote the transport of electrons. The contained N and O atoms enhance the binding of PACS with Li⁺ and, to some extent, improve the lithium storage. Especially, the ultrathin carbon shell greatly shortens the pathway of Li⁺ and the macropores virtually act as reservoirs for the electrolyte, ensuring efficient Li⁺ insertion into the carbon shells from both the outer and inner sides. With the unique and novel structure, PACS as the anode electrode material for LIBs has a high electrochemical performance.

4. Conclusions

In summary, we demonstrated a facile template-assisted method to prepare PACS from petroleum asphalt, which showed high reversible capacity and enhanced cycling property as anode material of LIBs, owing to four aspects: (1) unique hollow structure plays an essential role of ion-buffering reservoirs thus making sure that almost every part of the PACS could sufficiently touch electrolyte; (2) ultrathin porous shells (4.7 nm) shorten the Li⁺

diffusion path to less than 2.5 nm; (3) the high level of disorder degree provides extra lithium storage sites; (4) the contained nitrogen atoms promote the chemical reactivity and binding ability of PACS with lithium ions. All in all, with rational and delicate design, high reversible capacity and reliable cycling property, PACS shows a promising application future as electrode material for LIBs.

Acknowledgements

This work was supported by the National Natural Science Foundation of China (Nos. 51372028, 21302224, 51372277); the Fundamental Research Fund for the Central Universities (No. 15CX08005A).

Appendix A. Supplementary data

Supplementary data associated with this article can be found, in the online version, at <http://dx.doi.org/10.1016/j.cej.2015.10.102>.

References

- [1] D.W. Han, S.J. Lim, Y.I. Kim, S.H. Kang, Y.C. Lee, Y.M. Kang, Facile lithium ion transport through superionic pathways formed on the surface of Li₃V₂(PO₄)₃/C for high power Li ion battery, *Chem. Mater.* 26 (2014) 3644–3650.
- [2] W. Wang, C. Yu, Y. Liu, J. Hou, H. Zhu, S. Jiao, Single crystalline Na₂Ti₃O₇ rods as an anode material for sodium-ion batteries, *RSC Adv.* 3 (2013) 1041–1044.
- [3] M.S. Park, G.X. Wang, Y.M. Kang, D. Wexler, S.X. Dou, H.K. Liu, Preparation and electrochemical properties of SnO₂ nanowires for application in lithium-ion batteries, *Angew. Chem. Int. Ed.* 46 (2007) 750–753.
- [4] F.D. Han, Y.J. Bai, R. Liu, B. Yao, Y.X. Qi, N. Lun, J.X. Zhang, Template-free synthesis of interconnected hollow carbon nanospheres for high-performance anode material in lithium-ion batteries, *Adv. Energy Mater.* 1 (2011) 798–801.
- [5] J. Cabana, L. Monconduit, D. Larcher, M. Rosa Palacin, Beyond intercalation-based li-ion batteries: the state of the art and challenges of electrode materials reacting through conversion reactions, *Adv. Mater.* 22 (2010) E170–E192.
- [6] M. Rosa Palacin, Recent advances in rechargeable battery materials: a chemist's perspective, *Chem. Soc. Rev.* 38 (2009) 2565–2575.
- [7] B.J. Landi, M.J. Ganter, C.D. Cress, R.A. DiLeo, R.P. Raffaele, Carbon nanotubes for lithium ion batteries, *Energy Environ. Sci.* 2 (2009) 638–654.
- [8] H.Y. Wang, T. Abe, S. Maruyama, Y. Iriyama, Z. Ogumi, K. Yoshikawa, Graphitized carbon nanobeads with an onion texture as a lithium-ion battery negative electrode for high-rate use, *Adv. Mater.* 17 (2005) 2857–2860.
- [9] H.S. Zhou, S.M. Zhu, M. Hibino, I. Honma, M. Ichihara, Lithium storage in ordered mesoporous carbon (CMK-3) with high reversible specific energy capacity and good cycling performance, *Adv. Mater.* 15 (2003) 2107–2111.
- [10] D. Pan, S. Wang, B. Zhao, M. Wu, H. Zhang, Y. Wang, S. Jiao, Li storage properties of disordered graphene nanosheets, *Chem. Mater.* 21 (2009) 3136–3142.
- [11] Z.J. Fan, J. Yan, T. Wei, G.Q. Ning, L.J. Zhi, J.C. Liu, D.X. Cao, G.L. Wang, F. Wei, Nanographene-constructed carbon nanofibers grown on graphene sheets by chemical vapor deposition: high-performance anode materials for lithium ion batteries, *ACS Nano* 5 (2011) 2787–2794.
- [12] B.M. Tien, M.W. Xu, J.F. Liu, Synthesis and electrochemical characterization of carbon spheres as anode material for lithium-ion battery, *Mater. Lett.* 64 (2010) 1465–1467.
- [13] K. Wang, Z. Li, Y. Wang, H. Liu, J. Chen, J. Holmes, H. Zhou, Carbon nanocages with nanographene shell for high-rate lithium ion batteries, *J. Mater. Chem.* 20 (2010) 9748–9753.
- [14] Y. Wang, F.B. Su, J.Y. Lee, X.S. Zhao, Crystalline carbon hollow spheres, crystalline carbon-SnO₂ hollow spheres, and crystalline SnO₂ hollow spheres: synthesis and performance in reversible Li-ion storage, *Chem. Mater.* 18 (2006) 1347–1353.
- [15] C. Xu, G. Ning, X. Zhu, G. Wang, X. Liu, J. Gao, Q. Zhang, W. Qian, F. Wei, Synthesis of graphene from asphaltene molecules adsorbed on vermiculite layers, *Carbon* 62 (2013) 213–221.
- [16] I.F. Cheng, Y. Xie, R.A. Gonzales, P.R. Breyne, J.P. Sundararajan, B.A.F. Kengne, D. E. Aston, D.N. McLroy, J.D. Foutch, P.R. Griffiths, Synthesis of graphene paper from pyrolyzed asphalt, *Carbon* 49 (2011) 2852–2861.
- [17] J.R. Matos, M. Kruk, L.P. Mercuri, M. Jaroniec, L. Zhao, T. Kamiyama, O. Terasaki, T.J. Pinnavaia, Y. Liu, Ordered mesoporous silica with large cage-like pores: structural identification and pore connectivity design by controlling the synthesis temperature and time, *J. Am. Chem. Soc.* 125 (2003) 821–829.
- [18] D.C. Guo, F. Han, A.H. Lu, Porous carbon anodes for a high capacity lithium-ion battery obtained by incorporating silica into benzoxazine during polymerization, *Chem. Eur. J.* 21 (2015) 1520–1525.
- [19] Y.P. Wu, E. Rahm, R. Holze, Carbon anode materials for lithium ion batteries, *J. Power Sources* 114 (2003) 228–236.
- [20] Z.H. Ni, H.M. Wang, J. Kasim, H.M. Fan, T. Yu, Y.H. Wu, Y.P. Feng, Z.X. Shen, Graphene thickness determination using reflection and contrast spectroscopy, *Nano Lett.* 7 (2007) 2758–2763.

- [21] H. Badenhorst, Microstructure of natural graphite flakes revealed by oxidation: limitations of XRD and Raman techniques for crystallinity estimates, *Carbon* 66 (2014) 674–690.
- [22] X. Meng, Y. Zhong, Y. Sun, M.N. Banis, R. Li, X. Sun, Nitrogen-doped carbon nanotubes coated by atomic layer deposited SnO₂ with controlled morphology and phase, *Carbon* 49 (2011) 1133–1144.
- [23] H.B. Wang, C.J. Zhang, Z.H. Liu, L. Wang, P.X. Han, H.X. Xu, K.J. Zhang, S.M. Dong, J.H. Yao, G.L. Cui, Nitrogen-doped graphene nanosheets with excellent lithium storage properties, *J. Mater. Chem.* 21 (2011) 5430–5434.
- [24] L. Wang, Y. Zheng, X. Wang, S. Chen, F. Xu, L. Zuo, J. Wu, L. Sun, Z. Li, H. Hou, Y. Songt, Nitrogen-doped porous carbon/Co₃O₄ nanocomposites as anode materials for lithium-ion batteries, *ACS Appl. Mater. Interfaces* 6 (2014) 7117–7125.
- [25] Y. Xia, W. Zhang, Z. Xiao, H. Huang, H. Zeng, X. Chen, F. Chen, Y. Gan, X. Tao, Biotemplated fabrication of hierarchically porous NiO/C composite from lotus pollen grains for lithium-ion batteries, *J. Mater. Chem.* 22 (2012) 9209–9215.
- [26] H.G. Wang, Y. Wang, Y. Li, Y. Wan, Q. Duan, Exceptional electrochemical performance of nitrogen-doped porous carbon for lithium storage, *Carbon* 82 (2015) 116–123.
- [27] K. Tang, R.J. White, X. Mu, M.-M. Titirici, P.A. van Aken, J. Maier, Hollow carbon nanospheres with a high rate capability for lithium-based batteries, *ChemSusChem* 5 (2012) 400–403.
- [28] M. Chen, C. Yu, S. Liu, X. Fan, C. Zhao, X. Zhang, J. Qiu, Micro-sized porous carbon spheres with ultra-high rate capability for lithium storage, *Nanoscale* 7 (2015) 1791–1795.
- [29] D. Cai, L. Ding, S. Wang, Z. Li, M. Zhu, H. Wang, Facile synthesis of ultrathin-shell graphene hollow spheres for high-performance lithium-ion batteries, *Electrochim. Acta* 139 (2014) 96–103.
- [30] R. Song, H. Song, J. Zhou, X. Chen, B. Wu, H.Y. Yang, Hierarchical porous carbon nanosheets and their favorable high-rate performance in lithium ion batteries, *J. Mater. Chem.* 22 (2012) 12369–12374.
- [31] G. Wu, Z. Li, W. Wu, M. Wu, Effects of calcination on the preparation of carbon-coated SnO₂/graphene as anode material for lithium-ion batteries, *J. Alloys Compd.* 615 (2014) 582–587.
- [32] S. Wang, Y. Xing, C. Xiao, X. Wei, H. Xu, S. Zhang, Hollow carbon-shell/carbon-nanorod arrays for high performance Li-ion batteries and supercapacitors, *RSC Adv.* 5 (2015) 7959–7963.
- [33] L. Qie, W.M. Chen, Z.H. Wang, Q.G. Shao, X. Li, L.X. Yuan, X.L. Hu, W.X. Zhang, Y. H. Huang, Nitrogen-doped porous carbon nanofiber webs as anodes for lithium ion batteries with a superhigh capacity and rate capability, *Adv. Mater.* 24 (2012) 2047–2050.
- [34] J. Zhang, B. Guo, Y. Yang, W. Shen, Y. Wang, X. Zhou, H. Wu, S. Guo, Large scale production of nanoporous graphene sheets and their application in lithium ion battery, *Carbon* 84 (2015) 469–478.
- [35] S. Yoon, S. Lee, S. Kim, K.W. Park, D. Cho, Y. Jeong, Carbon nanotube film anodes for flexible lithium ion batteries, *J. Power Sources* 279 (2015) 495–501.
- [36] F. Han, D. Li, W.C. Li, C. Lei, Q. Sun, A.H. Lu, Nanoengineered polypyrrole-coated Fe₂O₃@C multifunctional composites with an improved cycle stability as lithium-ion anodes, *Adv. Funct. Mater.* 23 (2013) 1692–1700.
- [37] S. Yang, X. Feng, L. Zhi, Q. Cao, J. Maier, K. Muellen, Nanographene-constructed hollow carbon spheres and their favorable electroactivity with respect to lithium storage, *Adv. Mater.* 22 (2010) 838–842.
- [38] X. Shen, D. Mu, S. Chen, B. Wu, F. Wu, Enhanced electrochemical performance of ZnO-loaded/porous carbon composite as anode materials for lithium ion batteries, *ACS Appl. Mater. Interfaces* 5 (2013) 3118–3125.